

NONLINEAR-OPTICAL PHENOMENA

https://doi.org/10.1070/QEL17597

Nonlinear absorption of laser radiation by aluminium particles in a potassium bromide matrix

A.S. Zverev, A.V. Kalenskii, G.E. Ovchinnikov, A.A. Zvekov, E.V. Galkina

Abstract. **Optical properties of a model pressed composite (potassium bromide matrix with incorporated ALEX aluminium powder) are experimentally investigated. It is shown that the spectral dependences of total transmittance and diffuse reflectance can be described with allowance for the presence of both individual aluminium nanoparticles and their aggregates with a characteristic radius of 133 nm in a sample. It is found that irradiation of a composite sample by a 1070-nm cw laser initiates nonlinear absorption of radiation by aluminium particles, which is detected by a change in the sample optical density. A model is proposed to describe the effect, which is based on the sample heating and temperature dependence of the optical characteristics of aluminium particles. The calculation results are in qualitative agreement with the observed changes in optical density; hence, the thermal mechanism of nonlinear absorption of electromagnetic radiation by metal particles is applicable to this model system.**

Keywords: *nonlinear absorption of radiation, laser radiation, aluminium, thermal mechanism.*

1. Introduction

Optical properties of metal nanoparticles and structures consisting of them have attracted the attention of researchers for a fairly long time. A comprehensive theory of absorption and scattering of electromagnetic radiation by metal nanoparticles has been developed [1, 2], which makes it possible to optimise the linear optical properties of systems based on these particles [3]. The effect of nonlinear absorption of radiation by metal nanoparticles [4–6] can be used to develop switching devices, capable of selecting radiation in intensity. The nonlinear optical characteristics of samples based on nanoparticles in a transparent matrix depend on the nature of the metal and matrix, the size and shape of nanoparticles, the radiation wavelength, and the pulse duration [4, 5]. A number of thermal mechanisms have been proposed to interpret the effect of nonlinear absorption of light by metal nanoparticles; these mechanisms are based on heating nanoparticles by radiation with the corresponding change in their optical characteristics [7–9].

Most of the studies devoted to the optical properties of metal nanoparticles were carried out using silver and gold nanoparticles for the following reasons: (i) their plasmonic absorption bands fall in the visible region [4–6] and (ii) well-approved techniques for synthesising nanoparticles of desired size have been developed [4]. The plasmonic absorption bands of aluminium nanoparticles lie in the UV spectral region [10], and epitaxial aluminium films with a peculiar structure can also exhibit plasmonic properties in the visible range [11]. A study using pulsed radiation of the first and second harmonics of neodymium laser revealed a pronounced effect of nonlinear absorption in the 'pentaerythritol tetranitrate–aluminium nanoparticles' system, which was detected by the optoacoustic method [12]. Naseri and Dorranian [13] obtained polyvinyl alcohol films with additives of aluminium nanoparticles and showed that aluminium additive increases the nonlinear absorption coefficient for stationary 532-nm light. Nonlinear absorption in aluminium nanoparticles obtained by ablation in carbon tetrachloride and chloroform was found in [14].

Aluminium particles are a convenient model object to study the thermal nonlinear absorption mechanisms for several reasons: the temperature and wavelength dependences of the refractive index of aluminium are known [15, 16]; aluminium nanoparticles are protected by an oxide shell, which makes them stable up to the melting point [17]; and, finally, there are available commercial samples of ultrafine-grained aluminium. The purpose of this work was to investigate experimentally the optical characteristics of pressed pellets of potassium bromide with aluminium nanoparticles, heated by a stationary laser beam, and interpret the obtained experimental data within the mechanism of thermal nonlinear absorption of light, based on the temperature dependence of the refractive index of metal. Potassium bromide was chosen to be a matrix transparent in the visible and IR regions; it is a well-pressed material with a cubic lattice, for which the temperature and spectral dependences of refractive index are known [18].

2. Experimental technique

The samples for photometric studies were pressed pellets of potassium bromide of special-purity grade, containing 0.05 and 0.025 wt % ALEX aluminium powder. The powder contains aggregates of nanoparticles with radii from 25 to 100 nm (the average particle radius is 60 nm); the size of separate aggregates may reach 1 μm [19]. Figure 1b shows a transmission electron microscopy (TEM) image of powder and a histogram of particle-size distribution (with aggregation disregarded). When preparing samples, previously ground potassium bromide was dried at a temperature of 250°C for 3 h in a muffle furnace, after which it was cooled in the furnace and

A.S. Zverev, A.V. Kalenskii, G.E. Ovchinnikov, A.A. Zvekov, E.V. Galkina
Kemerovo State University, ul. Krasnaya 6, Kemerovo, 650000 Russia; e-mail: kalenskyav@gmail.com

Received 15 June 2021
Kvantovaya Elektronika **51** (8) 712–717 (2021)
Translated by Yu.P. Sin'kov

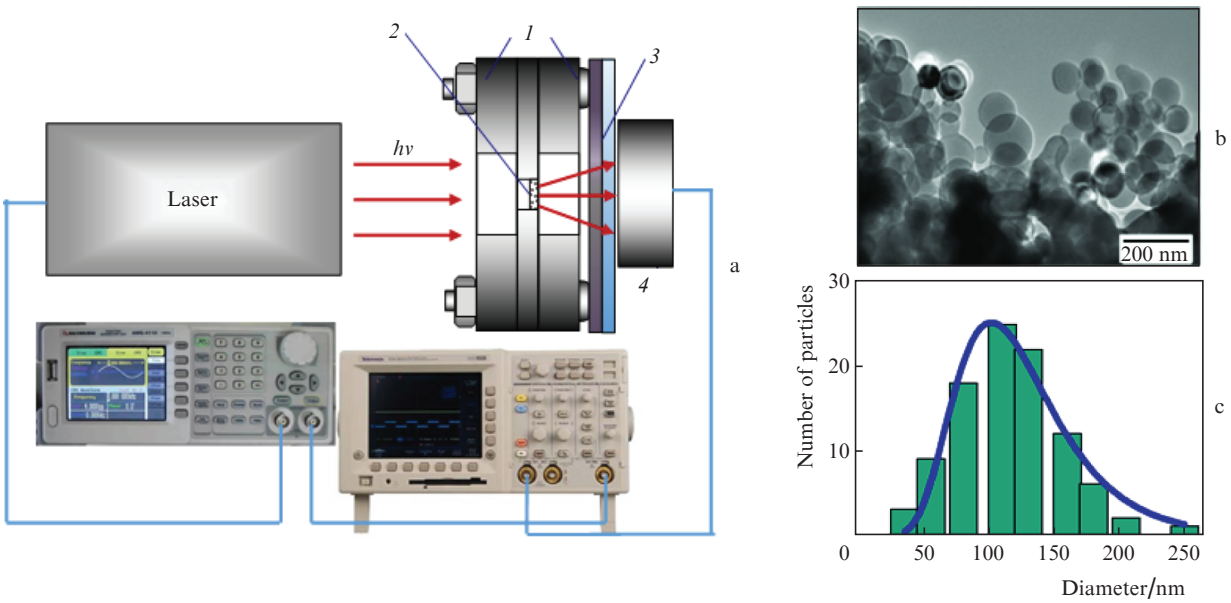

Figure 1. (a) Schematic of the experimental setup: (*1*) wafer for sample positioning in the holder; (*2*) sample; (*3*) light filters; (*4*) photodiode. (b) TEM image of powder and (c) particle-size distribution histogram, with aggregation disregarded.

in a desiccator to room temperature. The prepared KBr powder was mixed with aluminium powder by intense grinding in an agate mortar, until a mixture with an aluminium content of 1 wt % was formed. Then it was mixed in the same mortar with a necessary amount of potassium bromide to obtain mixtures with aluminium contents of 0.025 and 0.1 wt %, from which experimental samples 25 mm in diameter were pressed. Pressing was performed in a hydraulic press (OJSC LabTools, Russia) under a pressure of 1.2 GPa for 30 min. The sample mass was 400 ± 1 mg, and its thickness L was 300 ± 10 μm.

First we measured the linear optical characteristics of pellets of pure potassium bromide and pellets with aluminium additives, according to the technique reported in [20]. The total transmittance (diffuse and collimated components) and diffuse reflectance spectra in the wavelength range of 190–1500 nm was recorded using a scanning spectrophotometer Shimadzu UV-3600 (Shimadzu, Japan), equipped with an integrating sphere ISR-3100.

To study the nonlinear optical characteristics of aluminium particles exposed to laser radiation, we prepared pressed samples 3 mm in diameter (mass 6 mg, thickness 300 ± 10 μm). The samples were loaded in a steel holder in the same way as in [21]. A schematic of the experiment is shown in Fig. 1a. The radiation of ytterbium-doped fibre laser YLS-150/1500-QcW with a collimator IPG P30-001460 (wavelength 1070 nm) passed through a pellet and was recorded by a photodiode and a digital oscilloscope Tektronix TDS3032B (Tektronix, United States). The detector was located immediately adjacent to the assembly with a sample, which made it possible to determine the total intensity of transmitted radiation, including the diffuse component intensity. The laser effect duration in all measurements was 2 s. The laser pulse generation and oscilloscope launching were controlled by a digital pulse generator Aktakom AWG-4110 (Aktakom, Russia).

The change in the sample optical density (δA) in time was determined by subtracting the initial value (corresponding to the optical characteristics of samples at room temperature) from a signal.

3. Experimental results

The spectral dependences of total transmittance τ_t and diffuse reflectance ρ_d of potassium bromide free of aluminium additives are shown in Fig. 2a [curves (*1*) and (*2*)]. In the spectral range of 500–1500 nm the dependences are close to linear; the changes in τ_t and ρ_d are related to the wavelength dependence of light scattering coefficient from pores. The UV spectral region at $\lambda < 400$ nm is due to the potassium bromide absorption.

The measured total transmittance and reflectance spectra of KBr–Al samples with an aluminium mass fraction of 0.025% [Fig. 2b, curves (*1*) and (*2*)] have local extrema in the vicinity of 800 nm, which correspond to the interband absorption in aluminium [15, 16]. Aluminium particles efficiently absorb and scatter light in the entire spectral range under study, which leads to reduction of transmittance and increase in the diffuse reflectance in comparison with the corresponding parameters for a pure matrix.

The dependences of change in the optical density on the laser radiation exposure are presented in Fig. 3. Measurements were performed at four laser powers: 1.24 W (17.5 W cm^{-2}), 1.51 W (21.46 W cm^{-2}), 1.79 W (25.38 W cm^{-2}) and 3.02 W (42.65 W cm^{-2}). All dependences, except for that corresponding to the lowest laser beam intensity, have a maximum. The values of a maximum increase in the optical density almost coincide for the three highest laser powers. One can also observe coincidence of curves in their initial portions, a fact suggesting low-efficiency heat sink from the sample. The dependence recorded for the lowest power (1.24 W) tends to steady-state values during irradiation, which are much smaller than the maximum change in optical density observed at a higher laser power. At powers above 1.24 W the sample optical density decreased to values much lower than the initial ones. In this case, the sample underwent changes visible by the naked eye: It became more transparent, and one could select (in an optical microscope) the region of melting of not only aluminium but also potassium bromide.

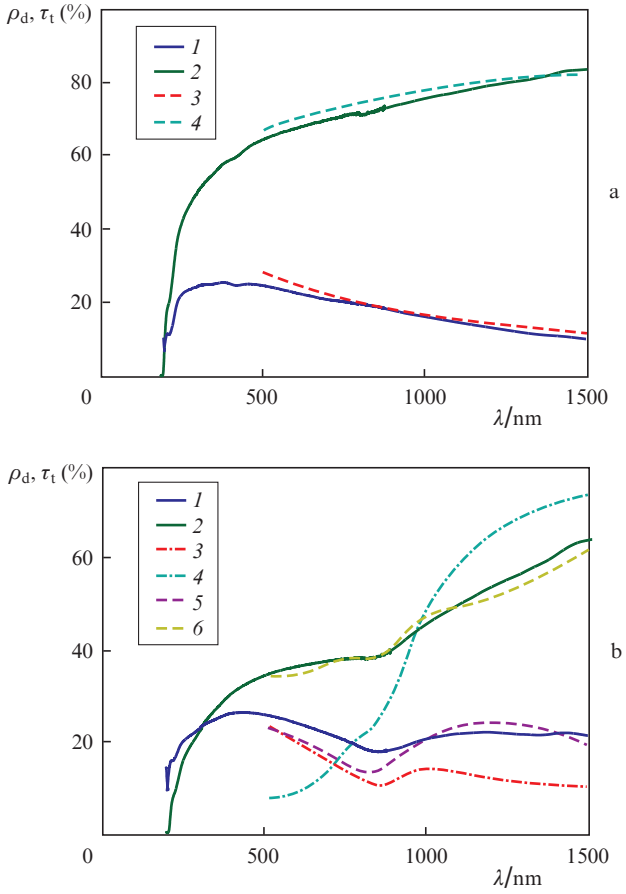

Figure 2. (*1*, *3*, *5*) Diffuse reflectance (ρ_d) and (*2*, *4*, *6*) total transmittance (τ_t) spectra of (a) pressed pellets of pure potassium bromide and (b) pellets with additive of ALEX aluminium particles (0.025 wt %): (*1*, *2*) experimental and (*3*–*6*) calculated curves.

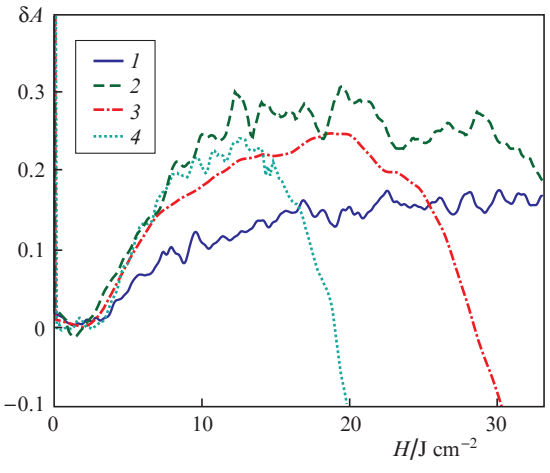

Figure 3. Dependences of the change in the sample optical density on the exposure to laser radiation with powers of (*1*) 1.24, (*2*) 1.51, (*3*) 1.79, and (*4*) 3.02 W.

4. Modelling of spectral dependences

The spectral dependences of total transmittance τ_t and diffuse reflectance ρ_d were modelled according to the technique proposed in [20]. To calculate the optical properties of aluminium particles [absorption efficiency (Q_{abs}) and scattering efficiency (Q_{sca}) factors, scattering phase function χ] within the Mie theory, we used the values of the complex refractive index of the metal [16] and potassium bromide [18]. Previously the dependences $\tau_t(\lambda)$ and $\rho_d(\lambda)$ were measured for pressed potassium bromide pellets without an aluminium additive. In this case, the attenuation of radiation is related to only its diffuse scattering from pores. The spectral dependence of the scattering coefficient of potassium bromide matrix was approximated by the expression

$$\mu_{KBr} = \mu_{KBr}^{(0)} \left(\frac{\lambda_0}{\lambda} \right)^b,$$

where the variable parameters are $\mu_{KBr}^{(0)}$ (the coefficient of scattering at wavelength $\lambda_0 = 500$ nm) and power b. The scattering phase function was specified in the Rayleigh form. The coefficients $\tau_t(\lambda)$ and $\rho_d(\lambda)$ were calculated using the one-dimensional monochromatic radiation transport equation [22, 23], which was solved with Fresnel boundary conditions by the spherical-harmonic method [20]. Twenty harmonics were used in the calculations. The calculation scheme was described in [20, 23]. A criterion for agreement between the calculated and experimental values was chosen to be the minimum of the sum of squared deviations. The sum was minimised applying the Nelder–Mead method. Numerical values for comparison were chosen in the spectral range of 500–1500 nm with a step of 50 nm. The best agreement was obtained for the parameters $\mu_{KBr}^{(0)} = 28.7$ cm^{-1} and $b = 1.093$ [Fig. 2a, curves (*3*, *4*)].

Figure 2b shows the calculated dependences $\tau_t(\lambda)$ and $\rho_d(\lambda)$ for a pressed pellet KBr–Al (0.025%) on the assumption that the average particle radius is 60 nm and the scattering coefficient μ_{KBr} is equal to the value for pure potassium bromide [curves (*3*, *4*)]. One can clearly see a significant difference between the calculated and experimental dependences. Consideration of the particle-size distribution does not improve the situation. An increase in the particle size diminishes the slope of the dependences $\tau_t(\lambda)$ and $\rho_d(\lambda)$. The effective size of particles can be increased as a result of their aggregation. When a pellet is pressed, some of pores are filled with aluminium particles [23], which leads to a decrease in the matrix scattering coefficient. In the next calculation cycle the variable parameters were taken to be the characteristic radius of aluminium-particle agglomerate, mass fraction of aggregates, and the ratio of the coefficient of scattering of potassium bromide in an aluminium-containing pellet to its value in pure KBr (relative coefficient of scattering). The calculation results obtained with optimal parameters (average aluminium aggregate radius 133 nm, mass fraction of aggregated particles 86% and matrix relative coefficient of scattering 0.157) are shown in Fig. 2b (curves *5* and *6*). Thus, the hypothesis about preservation of high degree of aluminium aggregation explains the character of obtained spectral dependences.

5. Model of change in the optical properties of radiation-heated sample

Heating of a pressed KBr–Al pellet by laser radiation leads to a change in its total transmittance. A schematic of this effect modelling is presented in Fig. 4.

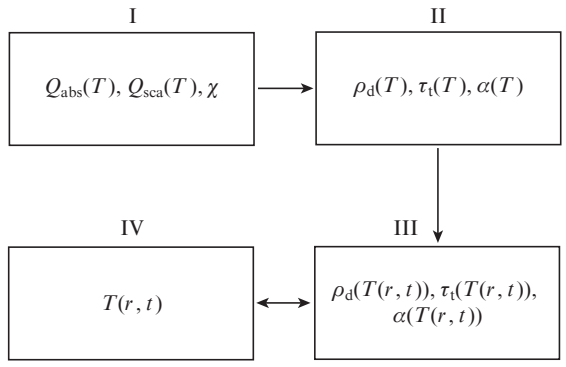

Figure 4. Schematic of the modelling of a change in sample optical density in the laser radiation field.

First, temperature dependences of the complex refractive indices of aluminium and potassium bromide were used to calculate the temperature dependences of the optical properties of aluminium particles with radii of 60 and 133 nm within the Mie theory (block I), from which local absorption and scattering coefficients of sample were determined. It was assumed that the matrix contribution to the coefficient of scattering does not change with an increase in temperature. The obtained dependences were applied to calculate (within the radiation transport theory in a plane-parallel layer of material in the approximation of infinitely wide beam) the temperature dependences of diffuse reflectance, transmittance, and absorptance, including the collimated and diffuse components (block II). Then the heating of potassium bromide pellet was calculated. At a mass fraction of aluminium particles of 0.1% and a characteristic radius of 133 nm, the particle concentration and the characteristic distance h between them can be estimated as 10^{10} cm^{-3} and ~1 μm, respectively. Heating of the potassium bromide region between particles occurs for a time $\lambda_{KBr}/(c_{KBr}\rho_{KBr}h^2) \approx 0.3$ μs, where $\lambda_{KBr} = 0.0418[1 - 10^{-3}(T - 273)]$ J cm^{-1} s^{-1} K^{-1} [24] is the potassium bromide specific thermal conductivity; T is temperature in kelvins; c_{KBr} is the specific heat, calculated based on the Shomate interpolation expression according to [25]; and $\rho_{KBr} = 2.75$ g/cm^{-3} is density. The thermal equilibrium settling times over the pellet thickness and radius can be estimated as $c_{KBr}\rho_{KBr}L^2/\lambda_{KBr} \approx 28$ ms and 700 ms, respectively. For this reason the heat conduction equation was solved in the one-dimensional approximation (block IV):

$$c_{KBr}\rho_{KBr}\frac{\partial T}{\partial t} = \lambda_{KBr}\left(\frac{\partial^2 T}{\partial r^2} + \frac{1}{r}\frac{\partial T}{\partial r}\right) + \alpha(T(r,t))\frac{W}{L},$$

where W is the laser power density on the sample, $\alpha(T(r,t))$ is the absorption coefficient, and r is radial coordinate. The sample was divided into 50 cells of constant width. The values $\alpha(T(r,t))$ in each cell were interpolated from the dependence $\alpha(T)$ (calculated in block II) at each integration step (block III). The bulky steel wafer was modelled as a cell 1 mm wide (an ideal thermal contact with the sample steel holder at the initial temperature). The chosen width provides close temperature-equalisation times in the steel wafer and neighbouring potassium bromide cells, despite the difference in thermal diffusivities. The calculation stopped when the maximum temperature reached the potassium bromide melting point.

6. Results of modelling of nonlinear absorption

The temperature dependence of the radiation absorption efficiency factor Q_{abs} for aluminium particles with a radius of 133 nm has a nonmonotonic character (Fig. 5). The wavelength of 1070 nm falls in the region between two interband absorption bands of bulk aluminium; in this case, according to the estimates of [15], the contribution of free electrons to optical conductivity is on the order of 30%. Slowdown of the increase in the imaginary part and simultaneous acceleration of the decrease in the real part of aluminium permittivity with an increase in temperature occur in the vicinity of $T = 590$ K, which gives rise to the maximum absorption efficiency factor (0.231). Near the melting point the absorption efficiency factor is even somewhat lower than at $T = 300$ K (0.149 and 0.170, respectively). Melting causes a sharp increase in Q_{abs}, after which the temperature dependence becomes close to linear. The scattering efficiency factor decreases in the entire temperature range. Within the interval from $T = 300$ K to the melting point, this decrease is 4.5%; upon melting, it amounts to 9.9%. Similar dependences were obtained previously for aluminium particles with a radius of 60 nm [16].

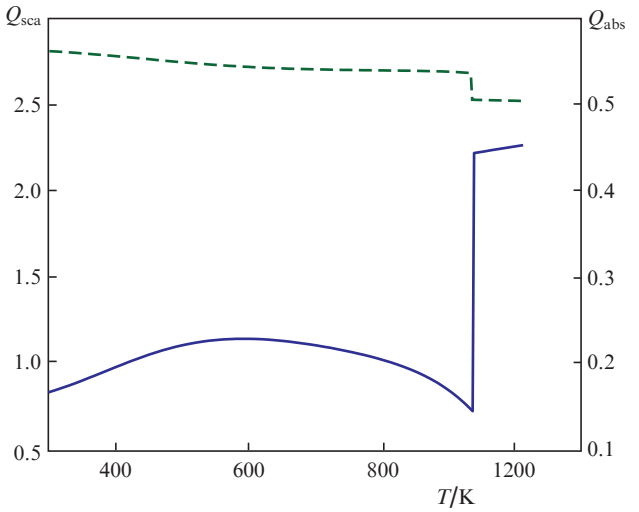

Figure 5. Calculated temperature dependences of the absorption efficiency factor Q_{abs} (solid line) and scattering efficiency factor Q_{sca} (dashed line); 1070-nm laser radiation, aluminium particles with a radius of 133 nm.

The calculated temperature dependence of the absorptance of a 300-μm-thick KBr pellet with a mass fraction of aluminium of 0.1% (Fig. 6) is qualitatively close to the dependence $Q_{abs}(T)$; however, the change in $\alpha(T)$ is less pronounced: it ranges from 0.570 at $T = 300$ K to 0.623 at $T = 590$ K. Similarly, the total transmittance decreases from 29.7% to 25.7% in the same temperature range, with a subsequent increase to 31.7% at the melting point. A change in temperature affects oppositely the diffuse reflectance and absorptance $\alpha(T)$, because the ρ_d value for optically dense samples is determined primarily by the single scattering albedo.

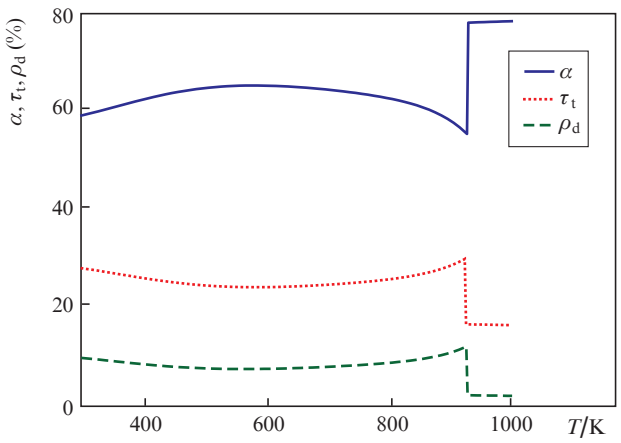

Figure 6. Calculated temperature dependences of the absorptance, transmittance, and reflectance of a 300-μm-thick KBr–Al sample with an aluminium mass fraction of 0.1%.

Figure 7a shows the calculated radial temperature distributions in the KBr–Al sample upon heating by 1070-nm laser radiation with a power of 1.79 W. The poor thermal contact results in large temperature values, whereas the heat sink at boundaries manifests itself in the maximum temperature at the sample centre and slowdown of the rise in temperature with time. The corresponding distributions of changes in the sample optical density are shown in Fig. 7b. Upon heating, the rise in temperature first leads to an increase and then to a decrease in optical density. Therefore, the point corresponding to the maximum δA value shifts from the centre of the sample to its periphery in the course of time. The calculated dependences of the temperature at the sample centre and the integral change in optical density on the pulse energy density are presented in Fig. 8. In all cases the temperature at the sample centre increases monotonically, and the dependences for the integral δA value have a maximum, which shifts to higher energy densities with increasing laser power. Recall that a similar shift of maximum was observed experimentally (Fig. 3). The calculated dependences demonstrate smaller maximum δA values, except for the dependence corresponding to a power of 1.24 W. The worst agreement between the calculation data and experimental results is observed for the highest power: 3.02 W. This disagreement is likely due to the pellet deformation (caused by thermal expansion), which may lead to formation of cracks.

Despite the aforementioned discrepancy between the experimental and modelling results, one can state that the change in the sample optical density is mainly related to the change in the optical properties of nanoparticles upon heating. Note that the modelling was performed using reference and published data, and the effective radius of aggregates was estimated from the results of spectral measurements.

7. Conclusions

It was shown experimentally that an exposure of composite sample to 1070-nm cw laser radiation initiates nonlinear absorption of this radiation by aluminium particles, which is related to sample heating. The revealed effect was interpreted within the thermal nonlinear absorption mechanism, which is based on the temperature dependence of optical constants of metal.

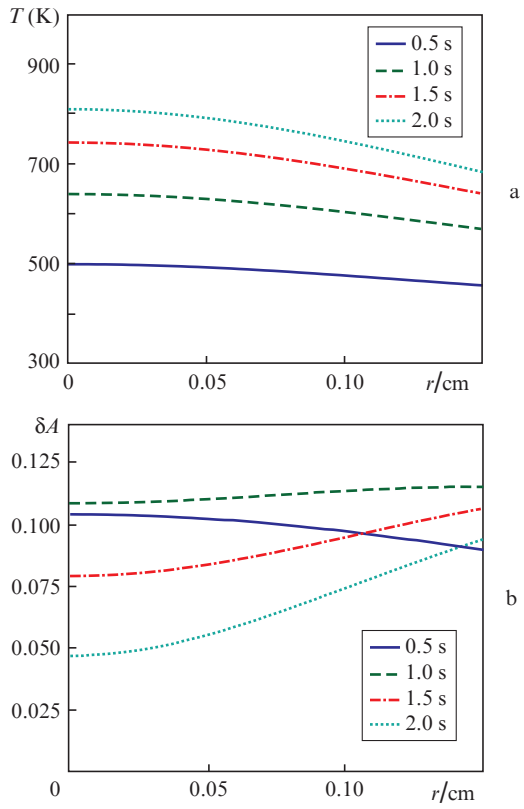

Figure 7. Calculated radial distributions of (a) temperature and (b) change in optical density in the KBr–Al (0.1 wt) sample for different calculation times.

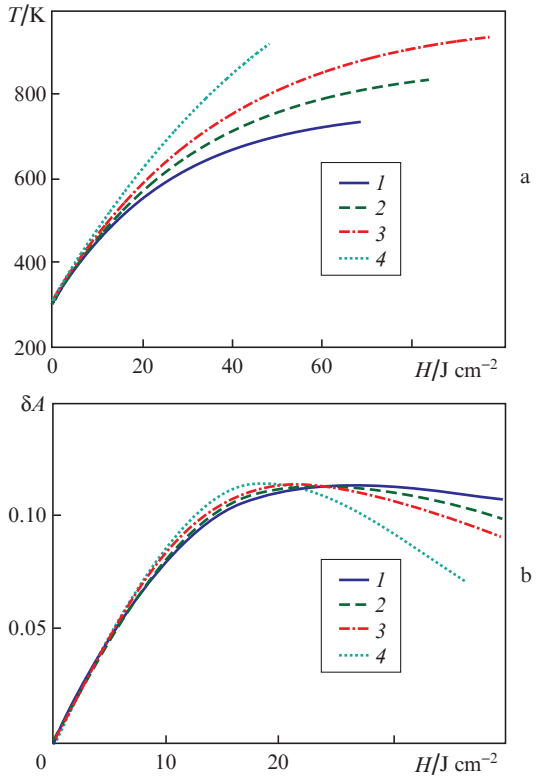

Figure 8. Calculated dependences of the (a) temperature at the pellet centre and (b) the integral change in optical density on the laser energy density H at powers of (*1*) 1.24, (*2*) 1.51, (*3*) 1.79, and (*4*) 3.02 W.

Acknowledgements. This work was supported by Grant No. MD-3502.2021.1.2 of the President of the Russian Federation.

References

1. Mie G. *Ann. Phys*., **330**, 377 (1908).
2. Shifrin S. *Rasseyanie sveta v mutnoi srede* (Light Scattering in a Turbid Medium) (Moscow–Leningrad: Gostekhizdat, 1951).
3. Klimov V.V. *Nanoplazmonika* (Nanoplasmonics) (Moscow: Fizmatlit, 2010).
4. Zhang Y., Wang Y. *RSC Advances*, **7**, 45129 (2017).
5. Ganeev R.A. *Opt. Spectrosc*, **127**, 487 (2019) [*Opt. Spektrosk*., **127**, 453 (2019)].
6. Zarate-Reyes J.M., Sanchez-Dena O., Flores-Romero E., Peralta-Angeles J.A., Reyes-Esqueda J.A., Cheang-Wong J.C. *Opt. Mater*., **111**, 110616 (2021).
7. Sivan Y., Chu S.-W. *Nanophotonics*, **6**, 317 (2017).
8. Un I.W., Sivan Y. *Phys. Rev. Mater.*, **4**, 105201 (2020).
9. Kalenskii A.V., Zvekov A.A., Nikitin A.P. *J. Appl. Spectrosc*., **83**, 1020 (2017) [*Zh. Prikl. Spektrosk*., **83**, 972 (2016)].
10. Knight M.W., King N.S., Liu L., Everitt H.O., Nordlander P., Halas N.J. *ACS Nano*, **8**, 834 (2014).
11. Cheng C.-W., Raja S.S., Chang Ch.-W., Zhang X.-Q., Liu P.-Y., Lee Y.-H., Shih Ch.-K., Gwo Sh. *Nanophotonics*, **10**, 627 (2021).
12. Aduev B.P., Nurmukhametov D.R., Belokurov G.M., Nelyubina N.V., Tupitsyn A.V. *Opt. Spectrosc.*, **124**, 412 (2018) [*Opt. Spektrosk*., **124**, 404 (2018)].
13. Naseri F., Dorranian D. *Opt. Quantum Electron*., **49**, 4 (2017).
14. Krishna Podagatlapalli G., Hamad S., Sreedhar S., Tewari S.P., Venugopal Rao S. *Chem. Phys. Lett*., **530**, 93 (2012).
15. Mathewson A.G., Myers H.P. *J. Phys. F: Met. Phys*., **2**, 403 (1972).
16. Kalenskii A.V., Zvekov A.A., Aduev B.P. *Opt. Spectrosc*., **124**, 501 (2018) [*Opt. Spektrosk*., **124**, 484 (2018)].
17. Vorozhtsov A.B., Lerner M., Rodkevich N., Nie H., Abraham A., Schoenitz M., Dreizin E.L. *Thermochim. Acta*, **636**, 48 (2016).
18. Li H.H. *J. Phys. Chem. Ref. Data*, **5**, 329 (1976).
19. Yang Y., Sun Zh., Wang Sh., Dlott D.D. *J. Phys. Chem. B*, **107**, 4485 (2003).
20. Aduev B.P., Nurmukhametov D.R., Belokurov G.M., Zvekov A.A., Kalenskii A.V., Nikitin A.P., Liskov I.Yu. *Tech. Phys*., **59**, 1387 (2014) [*Zh. Tekh. Fiz*., **84**, 126 (2014)].
21. Aduev B.P., Nurmukhametov D.R., Zvekov A.A., Liskov I.Yu., Belokurov G.M., Nelyubina N.V. *Tech. Phys*., **64**, 143 (2019) [*Zh. Tekh. Fiz*., **89**, 174 (2019)].
22. Ishimaru A. W*ave Propagation and Scattering in Random Media* (San Diego, California: Academic Press, 1978) Vol. 1.
23. Aduev B.P., Nurmukhametov D.R., Zvekov A.A., Nelyubina N.V., Sozinov S.A., Kalenskii A.V., Anan'eva M.V., Galkina E.V. *Opt. Spectrosc*., **128**, 664 (2020) [*Opt. Spektrosk*., **128**, 659 (2020)].
24. Kikoin I.K. (Ed.) *Tablitsy fizicheskikh velichin. Spravochnik* (Tables of Physical Values: A Handbook) (Moscow: Atomizdat, 1975).
25. Chase M.W. Jr; https://srd.nist.gov/JPCRD/jpcrdM9.pdf.